JOURNAL OF GEOPHYSICAL RESEARCH, VOL. 113, C12025, doi:10.1029/2008JC004908, 2008

Seasonal and interannual variations of upper ocean heat balance off the west coast of Australia

Ming Feng,[1] Arne Biastoch,[2] Claus Böning,[2] Nick Caputi,[3] and Gary Meyers[4]

Received 12 May 2008; revised 15 September 2008; accepted 23 September 2008; published 27 December 2008.

[1] The Leeuwin Current, a warm, poleward flowing eastern boundary current, dominates the surface circulation off the west coast of Australia and has profound influence on regional marine ecosystem and fisheries recruitment. In this study, the seasonal and interannual variations of upper ocean heat balance in the Leeuwin Current region are analyzed by using an eddy-resolving numerical model simulation, as a first step to quantify the climate impacts on regional ocean thermodynamics and marine ecosystem. The volume transport and heat advection of the Leeuwin Current are stronger during the austral winter on the seasonal cycle and are stronger during a La Nina event on the interannual scale. On both seasonal and interannual timescales, the mixed layer heat budget off the west coast of Australia is predominantly balanced between the variations of the Leeuwin Current heat advection and heat flux across the air-sea interface. On the interannual timescale, the variation of the Leeuwin Current heat advection tends to lead that of the air-sea (latent) heat flux by two months, which is likely a reflection of advection timescales of the Leeuwin Current and its eddy field. The interannual variation of the average February–April sea surface temperature off the west coast of Australia, which is crucial for the larval settlement of western rock lobster, is mostly influenced by the Leeuwin Current heat advection as well as the ocean memory from the previous austral winter, with the air-sea heat exchange playing a buffering role.

Citation: Feng, M., A. Biastoch, C. Böning, N. Caputi, and G. Meyers (2008), Seasonal and interannual variations of upper ocean heat balance off the west coast of Australia, *J. Geophys. Res.*, *113*, C12025, doi:10.1029/2008JC004908.

1. Introduction

[2] Ocean circulation off the west coast of Australia is dominated by the poleward flowing eastern boundary current, the Leeuwin Current. The Leeuwin Current originates from the North West Cape (22°S), and flows southward along the continental shelf break, being continually fed by onshore geostrophic flows. After arriving at the Cape Leeuwin (34°22′S, 115°08′E), the current turns eastward and enters the Great Australian Bight (Figure 1) [*Cresswell and Golding*, 1980]. The annual mean transport (geostrophic (referenced to 300 m) and Ekman transport) of the Leeuwin Current at 32°S is 3.4 Sv (1 Sv = 10^6 m^3 s^{-1}), as derived from historical data [*Feng et al.*, 2003]. The Leeuwin Current is stronger during the austral winter, with peak value of about 5 Sv during May–July, while it is weaker during the austral summer because of opposing southerly winds [*Godfrey and Ridgway*, 1985; *Smith et al.*, 1991]. On the interannual timescale, the strength of the Leeuwin Current is influenced by the El Niño/Southern Oscillation (ENSO) events because of the existence of the coastal waveguides through the Indonesian Archipelago and along the north and west Australian coasts (Figure 1) [*Meyers*, 1996]: the current is stronger during a La Niña event and weaker during an El Niño event [*Pearce and Phillips*, 1988; *Feng et al.*, 2003, 2005].

[3] Because of the existence of the Leeuwin Current, which carries warm and fresh tropical waters southward, the sea surface temperature (SST) off the west coast of Australia is 4–6°C warmer than typical upwelling eastern boundary systems at the same latitude [*Feng et al.*, 2003]. The Leeuwin Current has the strongest eddy kinetic energy among the midlatitude eastern boundary current systems [*Feng et al.*, 2005], thus the Leeuwin Current region in this study is defined as the area with strong mean flow and eddy energy between 110°E to the west coast of Australia. In a numerical model simulation, 70% of the Leeuwin Current heat advection is transferred to the ocean interiors by its eddy field, so that net ocean heat loss across the air-sea interface occurs in a broad region off the west coast of Australia [*Domingues et al.*, 2006]. On the interannual timescale, the net surface heat loss in the Leeuwin Current region is high during a La Nina event when the Leeuwin Current is strong, and low during an El Nino event with the Leeuwin Current is weak, as derived from the reanalysis products of numerical weather forecast models (M. Feng et al., Climate variability and ocean production in the Leeuwin

[1]CSIRO Marine and Atmospheric Research, Floreat, Western Australia, Australia.
[2]Leibniz-Institut für Meereswissenschaften, Kiel, Germany.
[3]Western Australian Fisheries and Marine Research Laboratories, Department of Fisheries, North Beach, Western Australia, Australia.
[4]Integrated Marine Observing System, University of Tasmania, Hobart, Tasmania, Australia.

0148-0227/08/2008JC004908$09.00

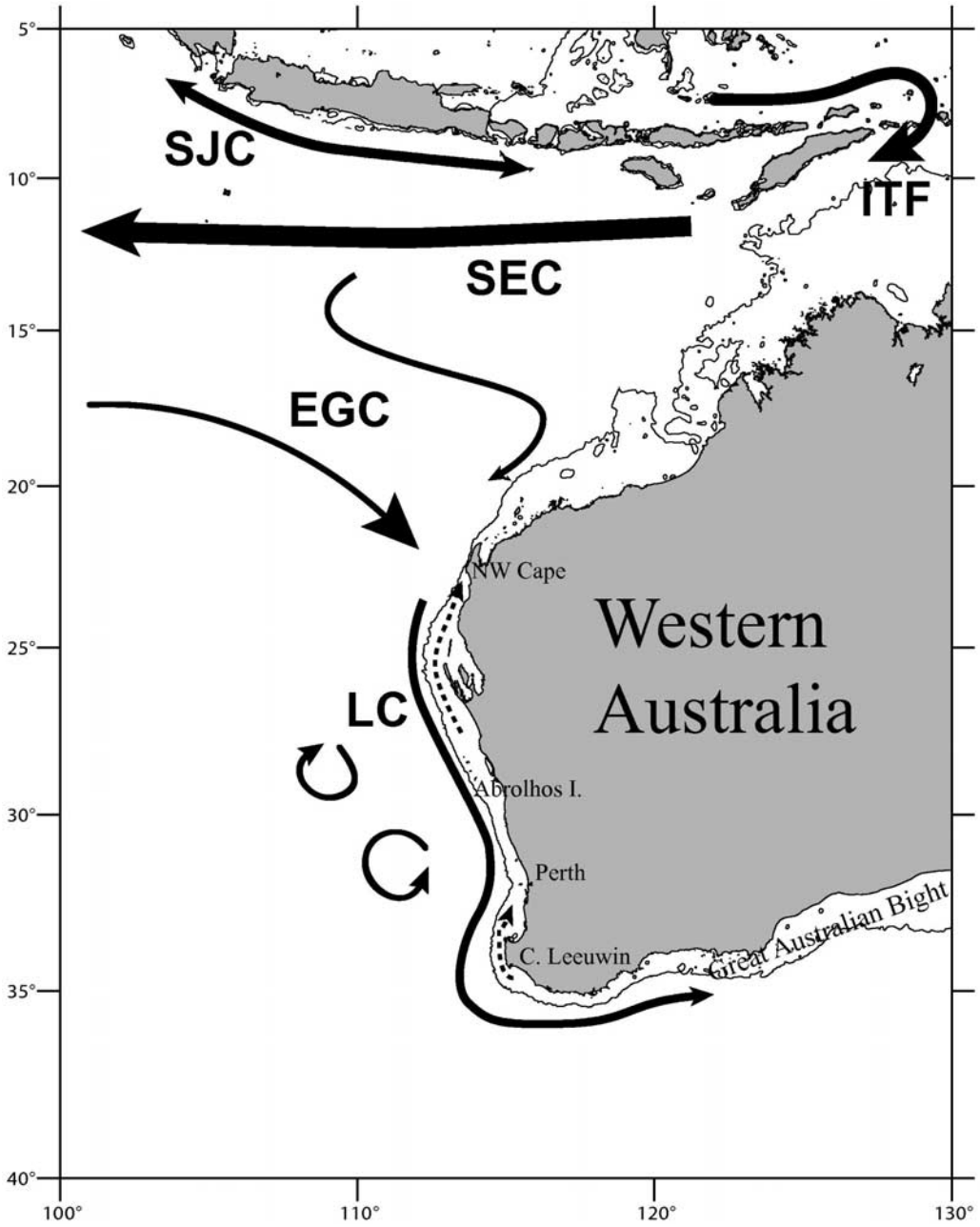

Figure 1. Regional surface currents in the East Indian Ocean and off the Western Austalian coast. ITF, Indonesian Throughflow; SJC, South Java Current; SEC, South Equatorial Current; EGC, East Gyral Current; LC, Leeuwin Current. The 200 m isobath of bottom bathymetry is shown as solid lines, and the dashed lines denote the inshore wind-driven currents during the austral summer.

Current off the west coast of Western Australia, submitted to *Journal of the Royal Society of Western Australia*, 2008). The interannual variation of February–April SST in the Leeuwin Current region is important to the larval settlement of western rock lobster, the most valuable single species fishery in Australia [*Caputi et al.*, 2001].

[4] In recent decades, increased warming rate of SST has been observed in the tropical Indian Ocean and in the Leeuwin Current region off the west coast of Australia [*Pearce and Feng*, 2007; *Alory et al.*, 2007; *Du and Xie*, 2008]. *Caputi et al.* [2008] have also shown that there are seasonal variations in the warming trend off the west coast of Australia, with most of the temperature increase occurring in the austral autumn-winter while little or no increase in the austral spring-summer. It is vital to understand the upper ocean thermodynamics in the Leeuwin Current region on different timescales, in order to improve our ability to understand the impacts of climate variability and climate change on the marine ecosystem off the west coast of Australia.

[5] In this study, the monthly output of a 45-year simulation (ORCA025-KAB001, hereafter called ORCA025)

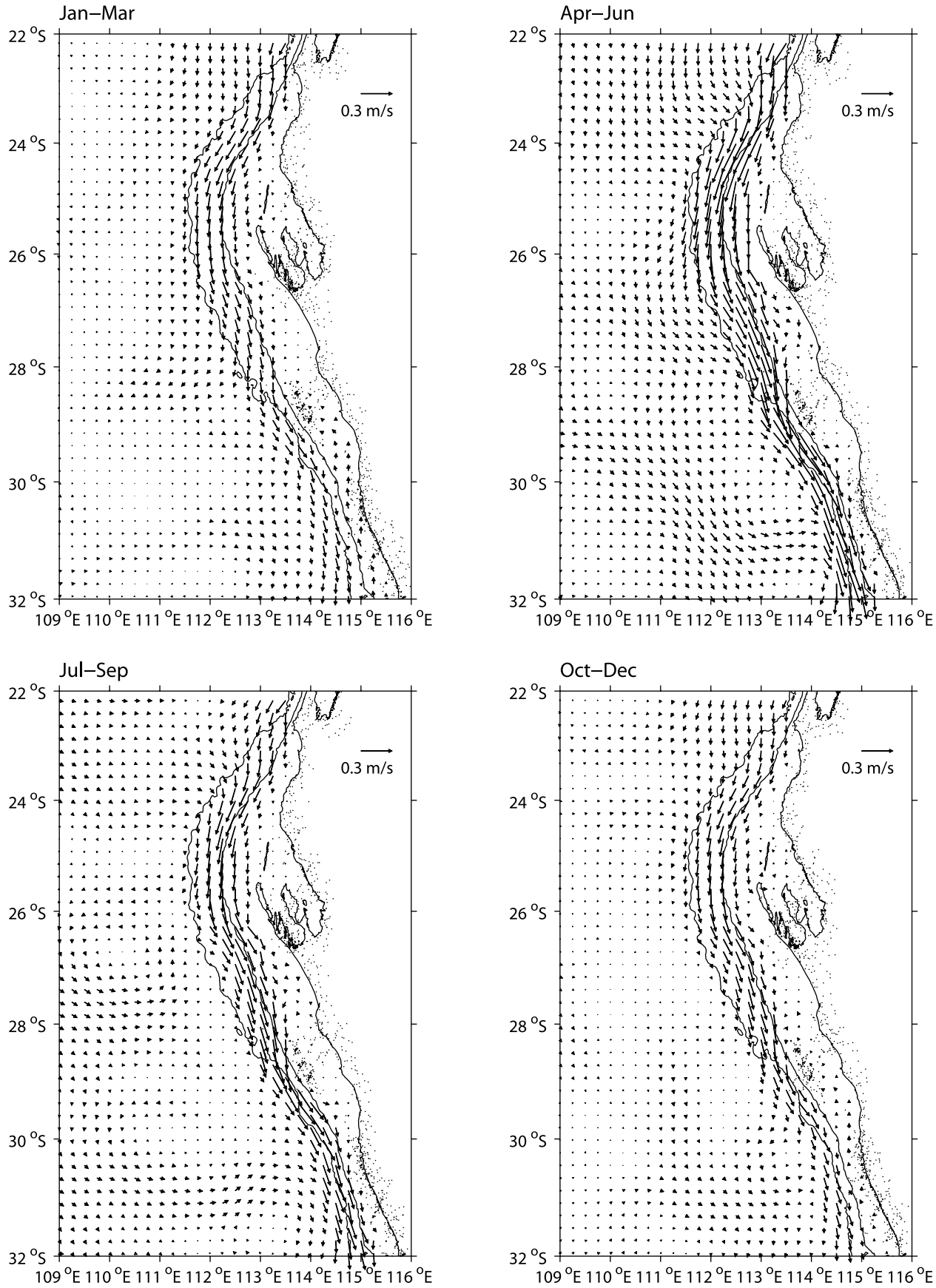

Figure 2. Seasonal averaged surface layer ocean current (upper 100 m) off the west coast of Australia from ORCA025. The 200 and 1000 m isobaths are shown as black contours.

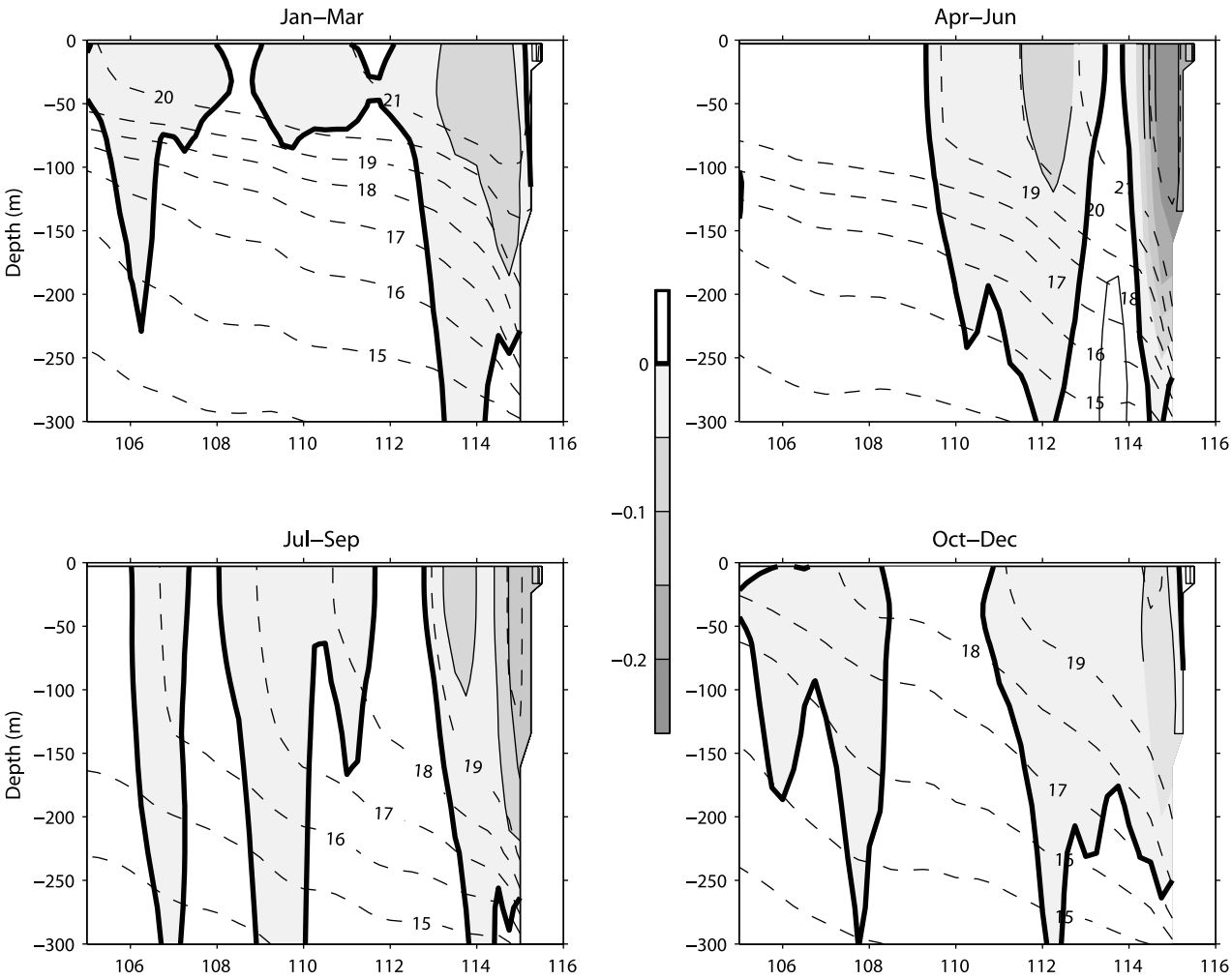

Figure 3. Seasonal averages of meridional velocity (shadings and solid contours) and temperature (dashed contours) in the upper 300 m at 32°S from ORCA025. Positive velocity (unshaded area) is northward, and the unit is m s^{-1}.

with a global eddy-resolving (0.25°) model is used to analyze the annual and interannual variations of the upper ocean heat balance in the Leeuwin Current region during the recent decades, as a first step to understand the SST variation and change in the region. Although there is a regional focus of this study, the method for heat budget calculation can be applied to other boundary current systems. The organization of the paper is as follows. In section 2, we introduce ORCA025 and the heat balance method. After evaluating the performance of ORCA025 in the Leeuwin Current region in section 3, the heat balance analyses on the seasonal and interannual timescales are presented in sections 4–6. The results are then summarized in section 7.

2. Data and Method

[6] ORCA025 is a global implementation of the OPA ocean model (the recent release 9.0 of the model described by *Madec* [2007], version of the NEMO model with nominal (longitudinal) grid sizes near the equator of 0.25°). The model has 46 geopotential levels of variable thickness; vertical resolution is 6m at the surface, and there are 20 vertical levels in the top 500 m. In the model, the lateral mixing is oriented along isopycnals. Topographic slopes are represented by a partial step formulation [*Adcroft et al.*, 1997]; together with an advanced energy-enstrophy conserving momentum advection scheme, the model configuration has been found to achieve significant improvements in simulating boundary currents and frontal regimes in the world oceans [*Barnier et al.*, 2006]. The momentum, heat and freshwater fluxes at the sea surface are implemented according to the CORE (Coordinated Ocean Reference Experiments) strategy, utilizing the bulk forcing methodology for global ocean ice models developed by *Large and Yeager* [2004]. It is based on NCEP/NCAR reanalysis products for the atmospheric state during 1958–2004, merged with various observational (e.g., satellite) products for radiation, precipitation and continental runoff fields, and adjusted so as to provide a globally balanced diurnal to decadal forcing ensemble [*Large*, 2007].

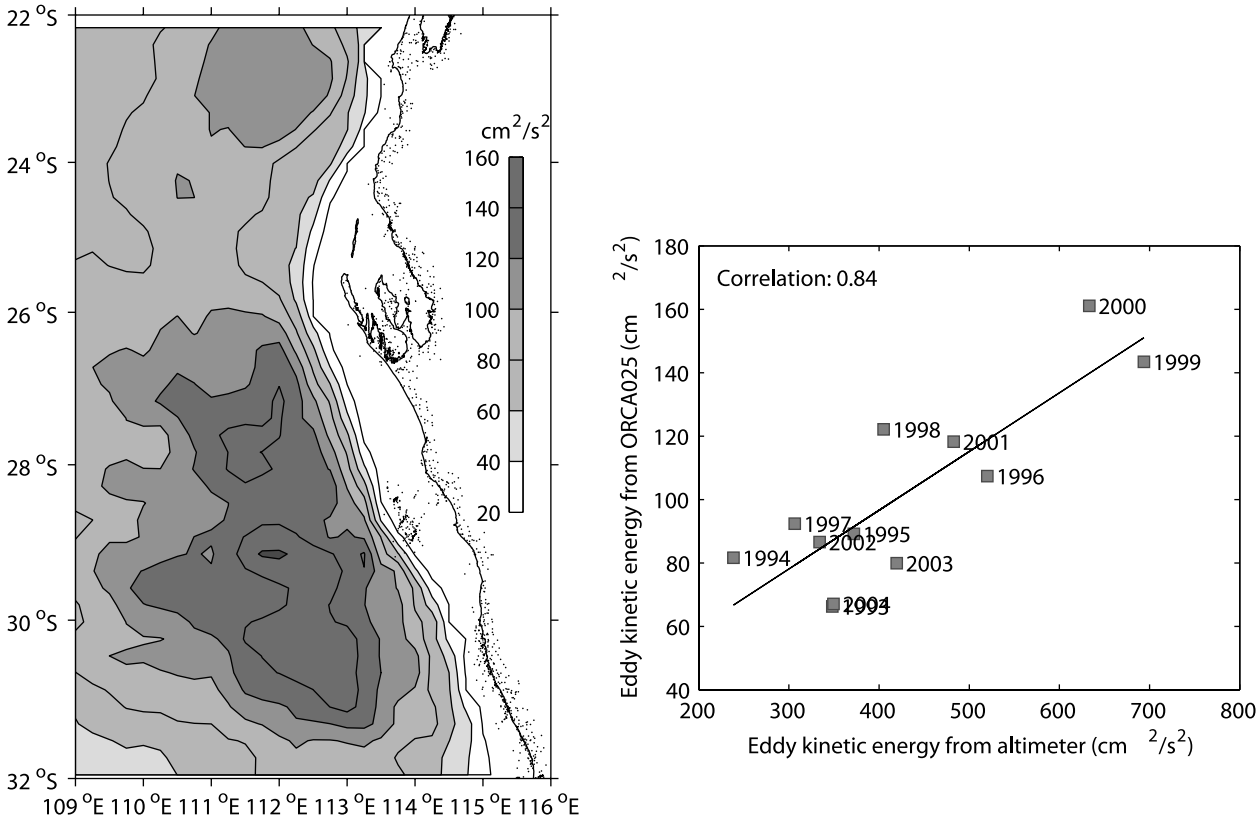

Figure 4. (left) Spatial distribution of surface kinetic energy derived from monthly ORCA025 output, and (right) a comparison of surface eddy kinetic energy average within 32–27°S, 110°E to the coast control box between ORCA025 output and altimeter data. The solid line in Figure 4 (right) shows the linear regression.

[7] Monthly values of horizontal velocity, temperature, latent and net air-sea heat flux from ORCA025 output at the 0.25° grid resolution are provided by Leibniz-Institut für Meereswissenschaften. The control volume of the upper ocean heat budget calculation is in the upper 7 levels of the model grid (from sea surface to about 58 m), within the horizontal domain of 32°S to 27°S and 110°E to the coast, with a total surface area of 2.52×10^{11} m^2. A spatial average vertical velocity at, h, the base of the control volume, is calculated by integrating the continuity equation within the control volume for each month:

$$\overline{w}|_{-h} = \left(-\iint_{110E} u dy dz + \iint_{27S} v dx dz - \iint_{32S} v dx dz \right) \Big/ \text{Area}$$

where u, v are zonal and meridional velocities. The heat budget is calculated by integrating the temperature equation

$$\frac{\partial T}{\partial t} + \frac{\partial u(T-T_0)}{\partial x} + \frac{\partial v(T-T_0)}{\partial y} + \frac{\partial w(T-T_0)}{\partial z} = \frac{1}{\rho c_P}\frac{\partial I}{\partial z} + \frac{\partial}{\partial z}\left(K_v \frac{\partial T}{\partial z}\right) + \nabla \cdot K_h \nabla T$$

within the control volume vertically from the sea surface to the base of the control volume, h,

$$\frac{\partial}{\partial t}\int_{-h}^{0} T dz + \frac{\partial}{\partial x}\int_{-h}^{0} u(T-T_0)dz + \frac{\partial}{\partial y}\int_{-h}^{0} v(T-T_0)dz - w|_{-h}\left(T|_{-h} - T_0\right) = \frac{Q_{net}}{\rho c_P} + R$$

and then horizontally

$$\rho c_P \frac{\partial}{\partial t}\iiint_V T dV = \text{ADV} + \iint_A Q_{net} dx dy + \rho c_P \iint_A R dx dy$$

$$\text{ADV} = -\rho c_P \left[-\iint_{110E} u(T-T_0) dy dz + \iint_{27S} v(T-T_0) dx dz - \iint_{32S} v(T-T_0) dx dz - \iint_{\text{Area}} w|_{-h}\left(T|_{-h} - T_0\right) dx dy \right]$$

where T is the model temperature and T_0 is the average temperature within the control volume, I is the penetrating solar radiation, and K_v and K_h are the vertical and horizontal diffusivities. Q_{net} is the net air-sea heat flux, including solar radiation and the turbulent fluxes. R is the residual, which

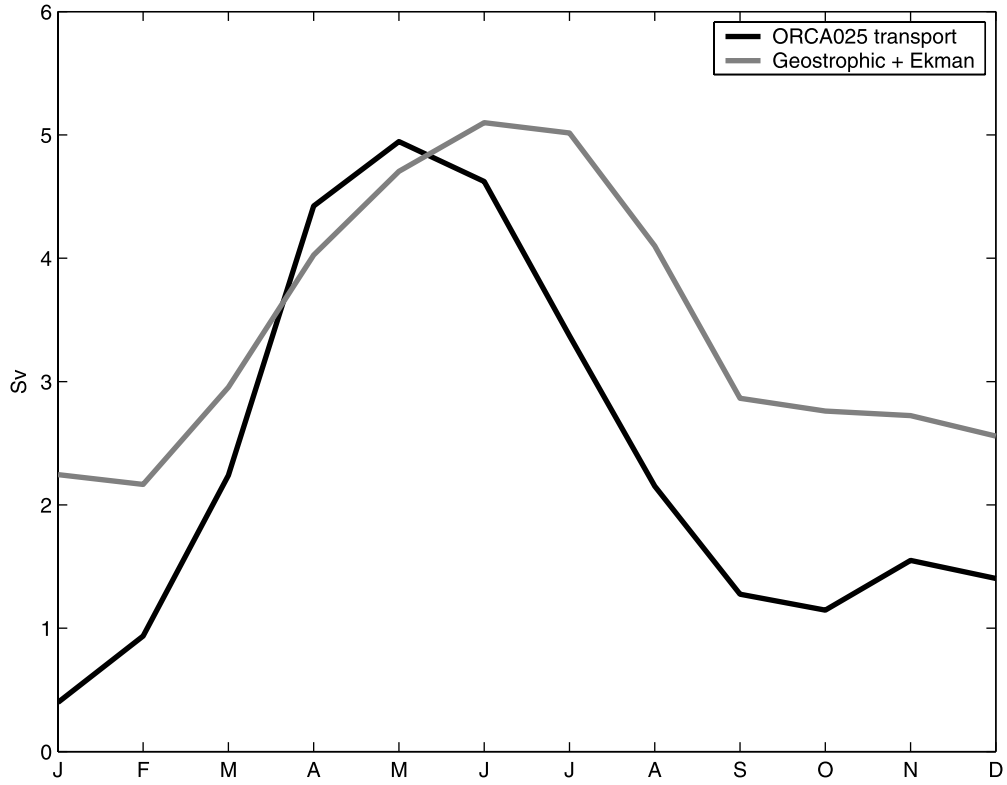

Figure 5. Monthly Leeuwin Current volume transports between 110°E and the coast at 32°S. The transport from ORCA025 is for the upper 248 m. The geostrophic transport is for the upper 300 m and referenced to 300 m, and the Ekman transport is derived from wind climatology [*Feng et al.*, 2003].

includes the penetrating solar radiation and vertical mixing at the base of the control volume and all other unresolved vertical and horizontal processes. Note that the selection of the open boundaries of the control volume avoids the high eddy kinetic region so that the effect of unresolved horizontal advection is minimized. ADV is the integration of the resolved heat advection terms at the three horizontal open boundaries and at the base of the control volume.

[8] Here T_0 is used as the reference temperature in the heat advection. Without T_0 in the heat advection, the reference temperature is in fact 0°, which is an arbitrary value. Change of reference temperatures will not affect the total advection, as long as the volume is conserved. However, without volume conservation, the advection term in a single direction becomes ambiguous. By adding the T_0 in the heat advection terms, the unbalanced volume flux in one direction is assumed to carry waters with the same temperature as T_0 so that it does not have a net contribution to the advection in that direction [*Lee et al.*, 2004].

[9] Two SST products are used to validate the spatially averaged model temperature in the Leeuwin Current region. The NOAA Extended Reconstruction of SST from 1854 (ERSST) [*Smith and Reynolds*, 2004] has a grid size of 2° and a timescale of a month. Weekly Tropical Rainfall Measuring Mission (TRMM) SST during 1998–2004 are obtained from Special Sensor Microwave/Imager (SSM/I) website [*Wentz*, 1997] and gridded into monthly averages. Monthly coastal sea levels at Fremantle (Perth), which are closely correlated to the Southern Oscillation Index [*Pearce and Phillips*, 1988] and linked to the strength of the Leeuwin Current [*Feng et al.*, 2003], are obtained from the National Tidal Centre, Bureau of Meteorology, Australia. Weekly sea surface height anomalies based on the combined TOPEX Poseidon (Jason-1) and ERS-1/ERS-2 (Envisat) satellite altimeter missions are obtained from CLS Space Oceanography Division [*Le Traon et al.*, 1998].

3. Model Simulation of the Leeuwin Current

[10] ORCA025 has reproduced the horizontal and vertical structures of the Leeuwin Current off the west coast of Australia (Figures 2 and 3). The modeled Leeuwin Current at 32°S is largely confined within the upper 300 m and the core of the mean current is along the shelf break, between 200 and 1000 m isobaths, consistent with current meter mooring observations [*Smith et al.*, 1991] and an upper ocean climatology derived from historical data [*Feng et al.*, 2003, 2005]. During 1960–2004, the average southward volume transport of the Leeuwin Current at 32°S (calculated for the upper 248 m (15 layers) and between 110°E and the coast) is 2.4 Sv, lower than that estimated from historical data [*Feng et al.*, 2003]. This is likely due to the stronger meridional wind forcing in ORCA025 compared with climatology [e.g., *Trenberth et al.*, 1989], by about 1 m s^{-1}, except in late autumn to early winter (not shown), as well as the low model resolution. The model also captures the Leeuwin Undercurrent at 250–800 m depth, with an average northward transport of 2.9 Sv between 110°E and the coast (not shown). The sea surface kinetic energy in the Leeuwin Current region is also lower in ORCA025 com-

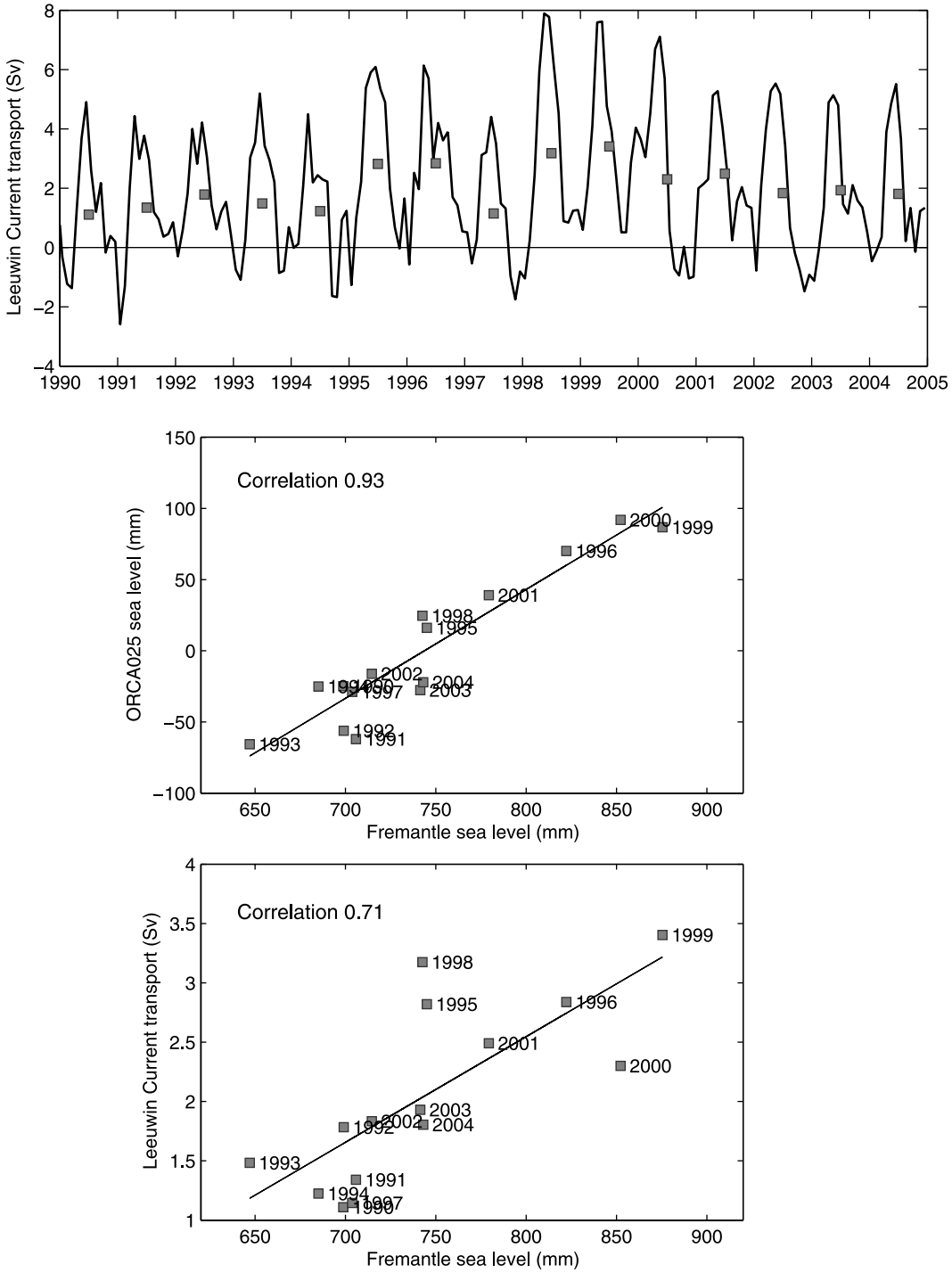

Figure 6. (top) Monthly Leeuwin Current transport at 32°S between 110°E and the coast derived from ORCA025 during 1990–2004 (squares denote annual averages). (middle) Relationship between annual mean Fremantle sea level from observation and from ORCA025. (bottom) Relationship between annual mean Fremantle sea level from observation and annual mean Leeuwin Current transport at 32°S from ORCA025. The solid lines are linear regressions between the variables in Figures 6 (middle) and 6 (bottom).

pared with that derived from satellite altimeter data (Figure 4 (left)) [*Reason et al.*, 1999; *Feng et al.*, 2005], but ORCA025 tends to capture the spatial distribution of the high eddy kinetic energy (Figure 4). The underestimate of the eddy energy is on one hand is because of the model resolution, and on the other hand is because of the fact that only the monthly averaged data are used for the calculation.

[11] The seasonal variations of the Leeuwin Current are also well simulated by ORCA025. In the surface layer, the

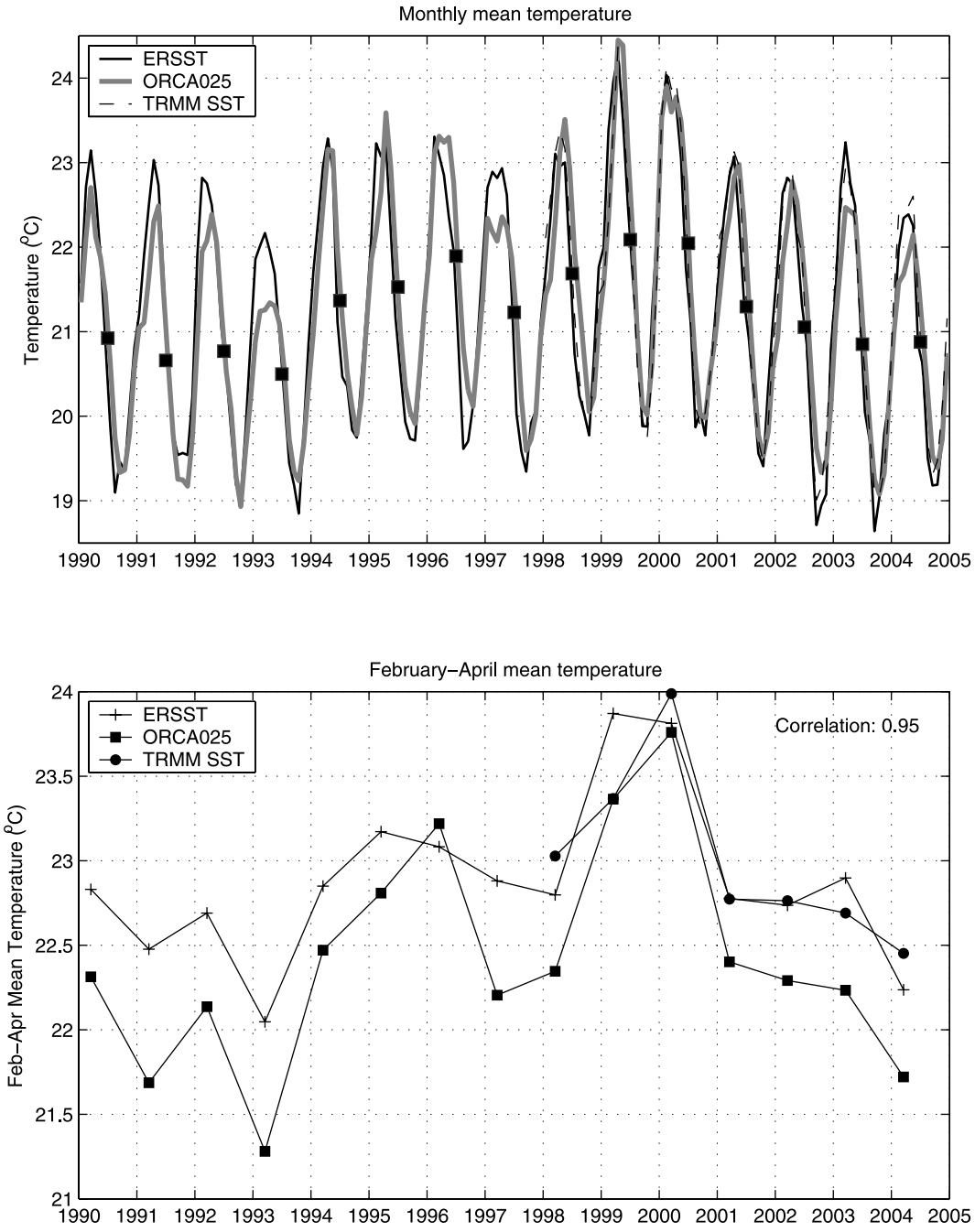

Figure 7. (top) Comparison of monthly ORCA025 SST (squares denote annual averages), ERSST, and Tropical Rainfall Measuring Mission SST. (bottom) February to April mean SSTs averaged in the region 32–27°S, 110°E to the coast during 1990–2004. Note that the ERSST has been reduced by 0.2°C to have the same average as the ORCA025 SST during this period.

current is fed by onshore flows off the upper west coast (north of 27°S) during the austral summer, while it is reinforced by onshore flows off both the upper and lower west coasts during the austral winter (Figure 2). The modeled southward transport off Perth reaches peak values during April–June, and there is a weak secondary peak in November (Figure 5). *Birol and Morrow* [2003] found a similar semiannual signal in tide gauge data along the west coast of Australia, which was suggested to be remotely forced in the tropical oceans. Further research is necessary to fully understand the mechanism of the semiannual variation. The underestimate of the Leeuwin Current transport mostly occurs during the austral summer, by about 50%, and there is a 1–2 month phase shift of the peak transport between ORCA025 and observation, which might be related to the meridional wind forcing of the model.

[12] There is significant interannual variation of the Leeuwin Current transport in ORCA025 (Figure 6). During 1990–2004, there are 4 years with above average transports, 1995, 1996, 1998, and 1999, and 9 years with below

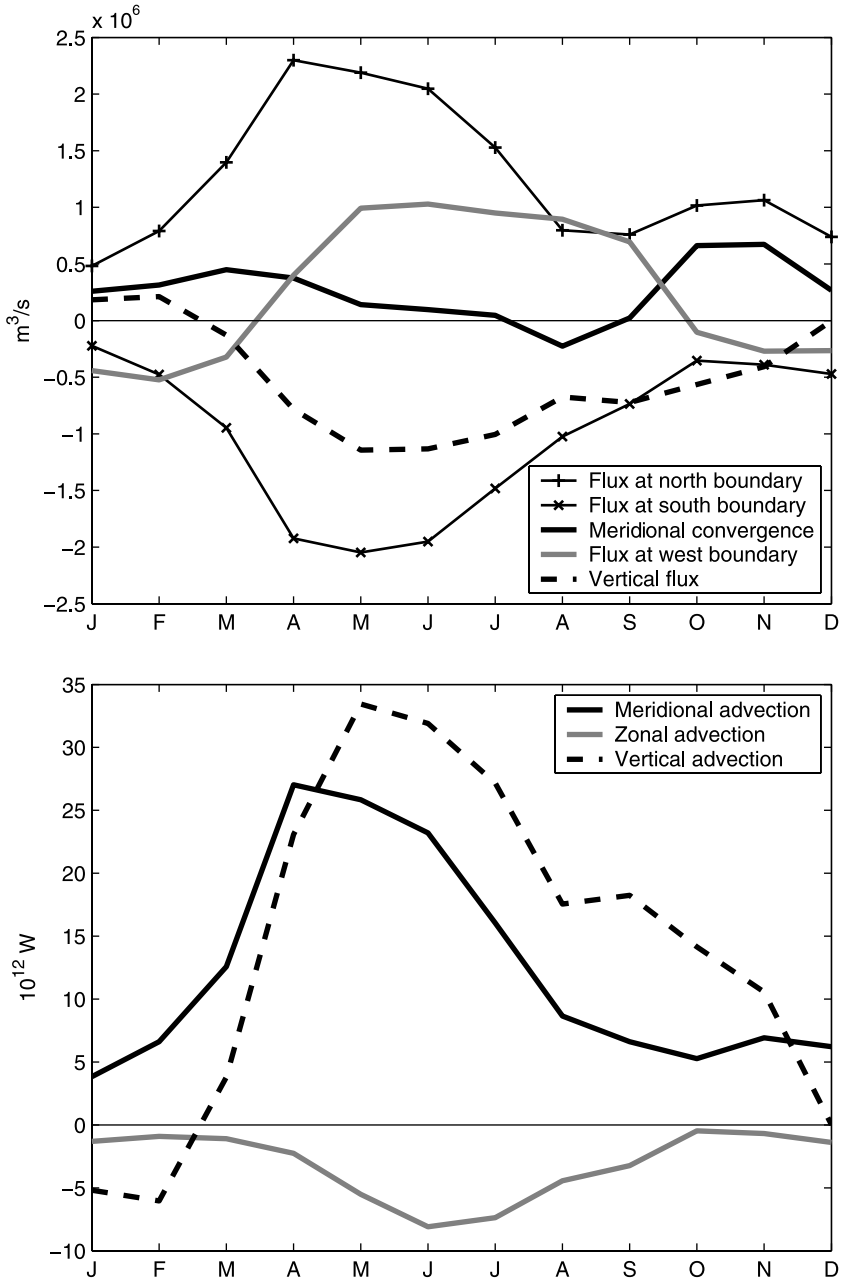

Figure 8. (top) Mean seasonal cycles of the volume fluxes into the control volume of the Leeuwin Current region at the north and south boundaries, the meridional convergence (the difference between the fluxes at the north and south boundaries), the flux at the west boundary, and the inferred vertical flux at the base of the control volume (~58 m). (bottom) Mean seasonal cycles of meridional, zonal, and vertical heat advections into the control volume. The positive values are volume fluxes into the control volume or supplying heat into the control volume.

average transports, 1990–1994, 1997, and 2002–2004. ORCA025 has reproduced most of the interannual variations of the Fremantle sea level (correlation 0.94), and the linear correlation between the annual mean transport of the Leeuwin Current and the Fremantle sea level is 0.71 (Figure 6 (bottom)). While most of the variability is related to the ENSO events during this period [*Feng et al.*, 2003], the relative high transports in 1995 and 1998 occur during the aftermath of two strong Indian Ocean Dipole events, which may have influenced the upper ocean heat content

Table 1. Annual Mean Convergence Rates for the Control Volume of Surface to 58 m, 32–27°S, 110°E to the Coast

Convergence Transport	Value
Meridional convergence (Sv)	0.26
Flux at north boundary	1.26
Flux at south boundary	−1.00
Zonal convergence (Sv)	0.25
Flux at west boundary	0.25
Flux at east boundary	0.00
Total convergence (Sv)	0.51
Vertical velocity at the base (10^{-6} m s^{-1})	−2.18

Table 2. Annual Mean Heat Balance Terms for the 32–27°S, 110°E to the Coast Region With Different Depth Ranges[a]

	Model Layers			
Model level	1–7	1–8	1–10	1–13
Depth range (m)	0–58	0–70	0–102	0–175
Surface heat flux (TW)	−19.7	−19.7	−19.7	−19.7
Total advection (TW)	23.4	30.4	48.0	56.7
Zonal	−3.1	−3.9	−6.3	−9.5
Meridional	12.4	14.7	18.9	21.2
Vertical	14.1	19.6	35.3	45.0
Residual (TW)	−3.7	−10.7	−28.3	−37.0

[a]Total surface area: 0.25×10^{12} m^2.

distribution and circulation off the northwest Australia [*Feng and Meyers*, 2003]. Note there is the record high transport of ~8 Sv in May 1998. The linkage between the strength of the Leeuwin Current and the Indian Ocean Dipole events has yet to be established. ORCA025 also captures most of interannual variation of the surface eddy kinetic energy, with a significant correlation of 0.84 with altimeter derived eddy kinetic energy during 1993–2004. 1999 and 2000 are confirmed to have the strongest eddy energetics in both model and altimeter data (Figure 4 (right)).

[13] The monthly SST from ORCA025 is significantly correlated with ERSST averaged over the control box off

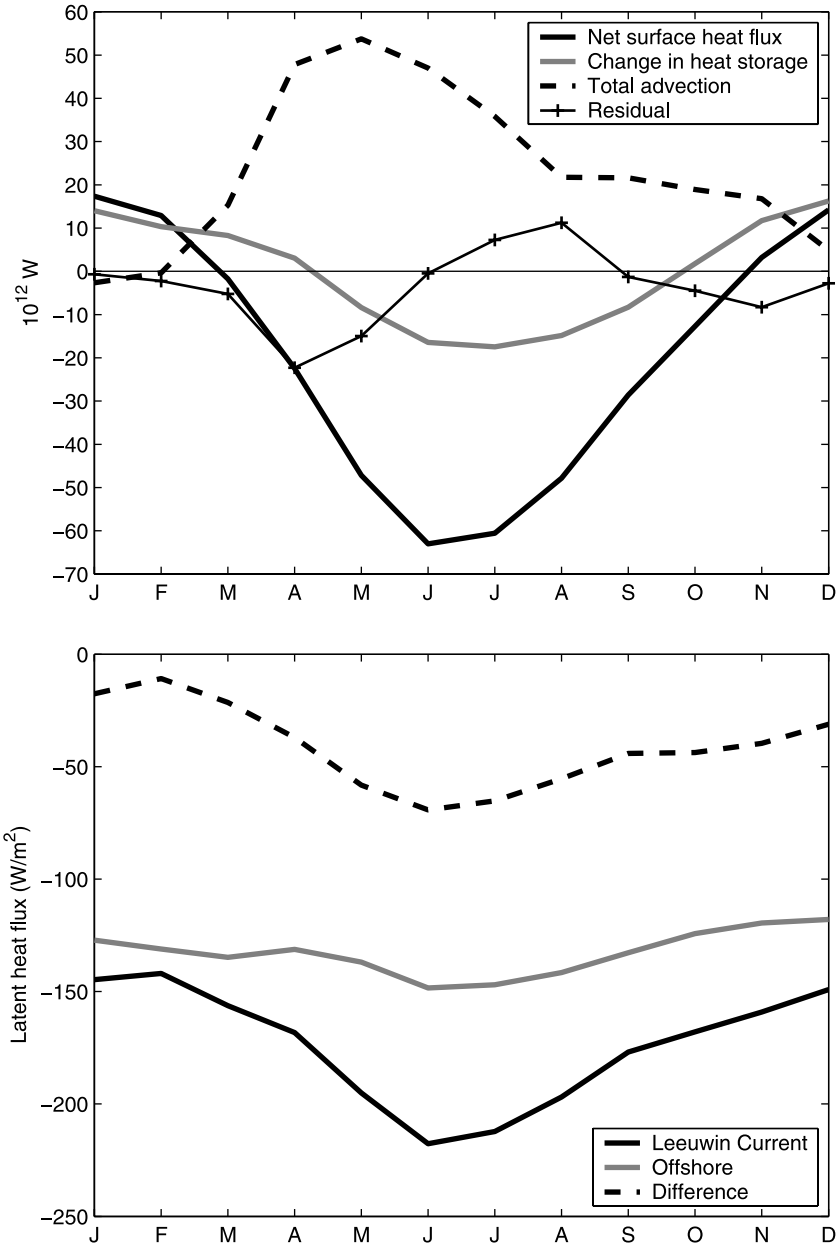

Figure 9. (top) Average monthly net air-sea heat flux, change in heat storage, total heat advection, and the residual term in the heat balance equation for the control volume in the Leeuwin Current region. (bottom) Average monthly surface latent heat flux in the Leeuwin Current control box, the offshore area of 32–27°S, 105–110°E, and their difference.

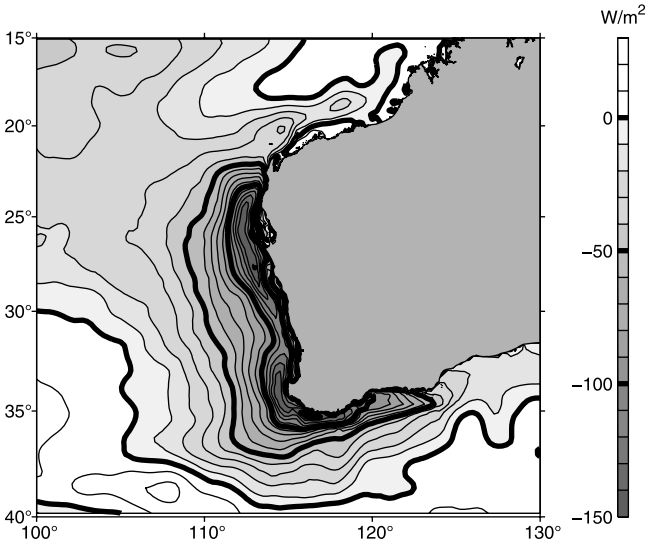

Figure 10. Net air-sea heat flux from ORCA025 during 1961–2004 (negative values denote areas where the ocean loses heat to the atmosphere).

the west coast of Australia on both seasonal and interannual timescales (there is a 0.2°C bias during the period of 1990–2004) (Figure 7 (top)). The TRMM SST during 1998–2004 is less biased and has similar seasonal and interannual variations (Figure 7). ORCA025 SST is less correlated with HadISST produced by the Met Office Hadley Centre [*Rayner et al.*, 2003]; and the difference between the ERSST and HadISST products in this region still needs to be fully understood.

[14] Although ORCA025 simulates a weaker Leeuwin Current compared to observation, the model captures the seasonal and interannual variations of Leeuwin Current in a consistent way. Thus, the model output is used to understand the upper ocean heat balances in the Leeuwin Current region on the seasonal and interannual timescales in the next sections.

4. Seasonal Cycle of the Heat Balance

[15] There is net convergence of surface water in the Leeuwin Current region off the west coast of Australia. The southward transports in the upper 58 m at the 27°S and 32°S sections are both stronger during the austral autumn and winter and weaker during the austral spring and summer, in phase with the seasonal cycle of the Leeuwin Current (Figure 8 (top); note that in Figure 8 positive flux is defined as flux into the control volume). The volume transport at 27°S is higher than that at 32°S, so that there is net convergence into the control volume in the meridional direction, with an annual mean value of 0.26 Sv (Table 1). The meridional convergence has two seasonal peaks, one in March and the other in October–November, likely related to the semiannual variation of the Leeuwin Current. The convergence due to zonal transport is positive during the austral winter when the meridional pressure gradient is stronger [*Godfrey and Ridgway*, 1985], while it is negative during the austral summer, with an annual mean net convergence of 0.20 Sv (Figure 8 (top)). By adding these two terms, downwelling is induced by the horizontal convergence all year-round except during the austral summer, and the annual mean vertical velocity is about 2×10^{-6} m s^{-1} averaged over the base of the control volume.

[16] Both the meridional and vertical temperature advection terms bring heat into the control volume (Figure 8 (bottom) and Table 2). The seasonal cycles of the meridional and the vertical advection terms follow the seasonal cycles of the volume fluxes, demonstrating the importance of the transport anomalies. The zonal advection carries a small amount of heat away from the control box. In sum, the total advection (ADV) brings heat into the control volume all year-round, with an annual mean contribution of 22.6 TW, peaking in April–May (Figure 9 (top)), when the modeled Leeuwin Current transport has its seasonal peak.

[17] On annual average, the upper ocean heat budget in the Leeuwin Current region is dominated by the two terms: the total advection which brings heat into this region and net air-sea heat flux which releases heat into the atmosphere (Figure 9 (top) and Table 2). The spatial structure of the long-term mean net air-sea flux from ORCA025 is similar to the *Large and Yeager* [2004] climatology (not shown), except that there is greater heat loss along the core of the Leeuwin Current in ORCA025 compared to the climatology (Figure 10), as ORCA025 better resolves the spatial structure of the Leeuwin Current compared to the climatology. During 1990–2004, the annual mean net air-sea heat loss averaged within the control volume is 19.7 TW (Table 2; 1 TW = 10^{12}W), or 78 W m^{-2}. On the seasonal cycle, the ocean loses heat to the atmosphere during April to October, while the ocean gains heat during the November–February (Figure 9 (top)). The peak heat loss occurs in June–July.

[18] About half of the heat input from the Leeuwin Current advection is released to the atmosphere through enhanced latent heat flux in the Leeuwin Current region (Figure 9 (bottom)). The latent heat fluxes in the Leeuwin Current and in the offshore region are phase locked in the seasonal cycle and the annual average of the difference between the two regions is 41 W m^{-2} (174 W m^{-2} in the Leeuwin Current and 133 W m^{-2} in the offshore region). Note most of the difference occurs after the strengthening of the Leeuwin Current in late autumn–early winter in the seasonal cycle, with peak value occurring in July, one month after the peak Leeuwin Current transport (Figure 9 (bottom)), presumably because of the increased SST contrast between the two regions.

[19] On annual average, the residual term has a small cooling contribution to the heat budget, −2.9 TW (Figure 9 (top) and Table 2), which is likely dominated by the penetrative solar radiation and vertical mixing across the base of the control volume. The residual is negative most of the year, except during the austral winter, when the mixed layer depth is deeper than the control volume depth (Figure 3) and the convective warming is expected to be important [*Shinoda and Hendon*, 2001].

[20] When using a deeper depth range to calculate the upper ocean heat budget, the total heat advection becomes a more dominant term, but the contribution from unresolved processes also becomes larger (Table 2). Thus, surface to 58 m (first 7 layers of model grid) is the optimal depth range for the heat budget calculation so that the residual is

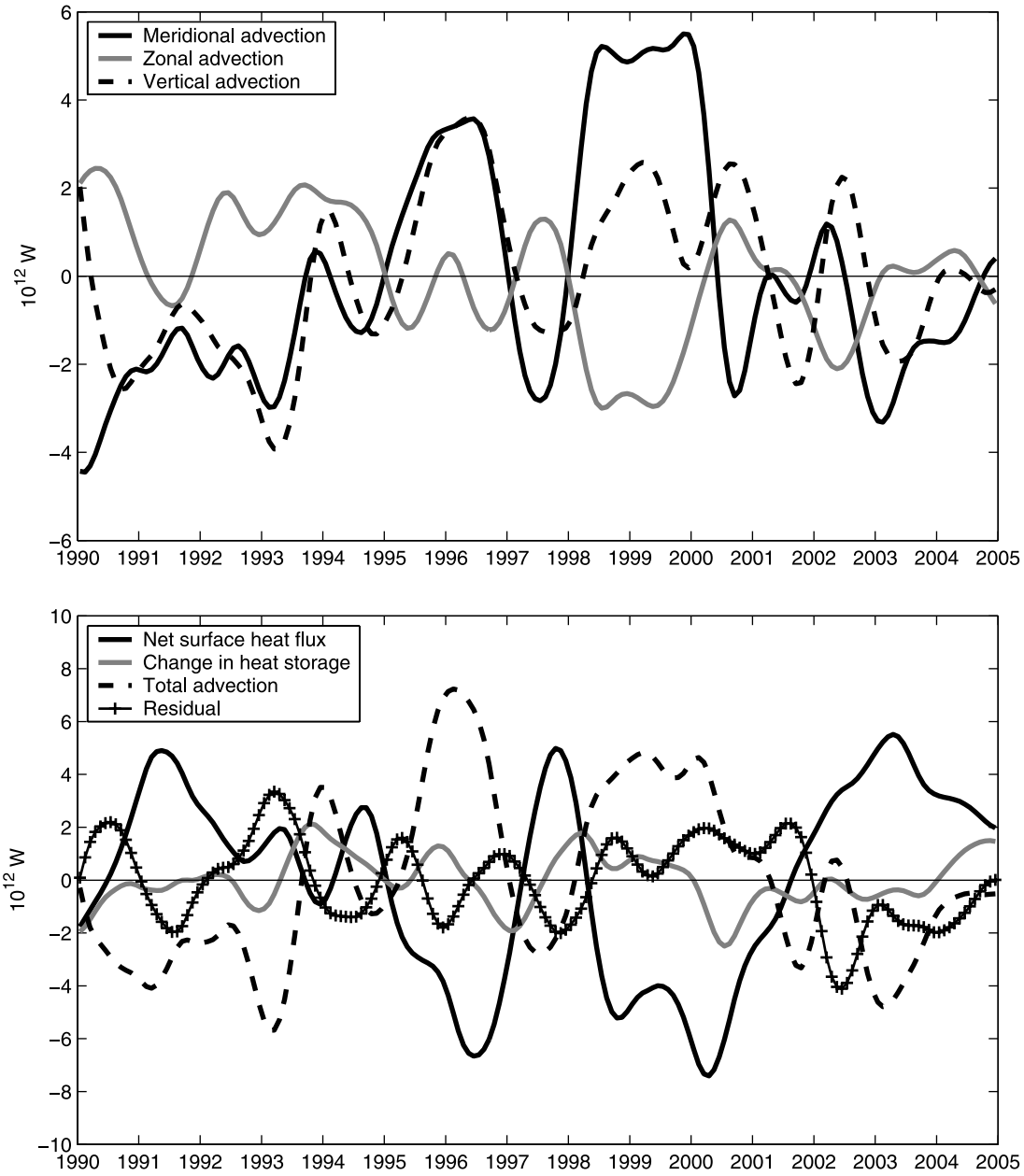

Figure 11. (top) Interannual anomalies of meridional, zonal, and vertical advection. (bottom) Interannual anomalies of net air-sea heat flux, change in heat storage, total advection, and residual of the upper ocean heat budget in the Leeuwin Current control volume during 1990–2004. All time series are smoothed with a 17-point Hanning filter.

minimized while the key upper ocean processes that affect SST are still captured. Note that 50 m is found to be the optimal depth as the base of the control volume for calculating heat budget in the equatorial western Pacific [*Feng et al.*, 1998].

5. Interannual Variation of Heat Balance

[21] The total heat advection and the air-sea heat flux are the two dominant terms in the interannual variation of the heat balance in the Leeuwin Current region. The interannual anomalies of meridional heat advection into the control volume are of the order of 5 TW and are positive when the Leeuwin Current is stronger, e.g., 1995–1996 and 1998–1999, and vice versa, e.g., 1990 and 1993 (Figure 11 (top)). Zonal advection anomalies are weaker and often have the opposite signs to the meridional advection anomalies, while the vertical advection anomalies often have the same signs as the meridional advection anomalies. Thus, the signs of the total heat advection anomalies are mostly determined by those of the meridional advection anomalies.

[22] In ORCA025, the interannual anomalies of the net surface heat flux into the ocean (Q_{net}) are negatively related with the total heat advection anomalies and the comparison of the two time series suggest that there is a two-month phase lag between the variations of the total heat advection

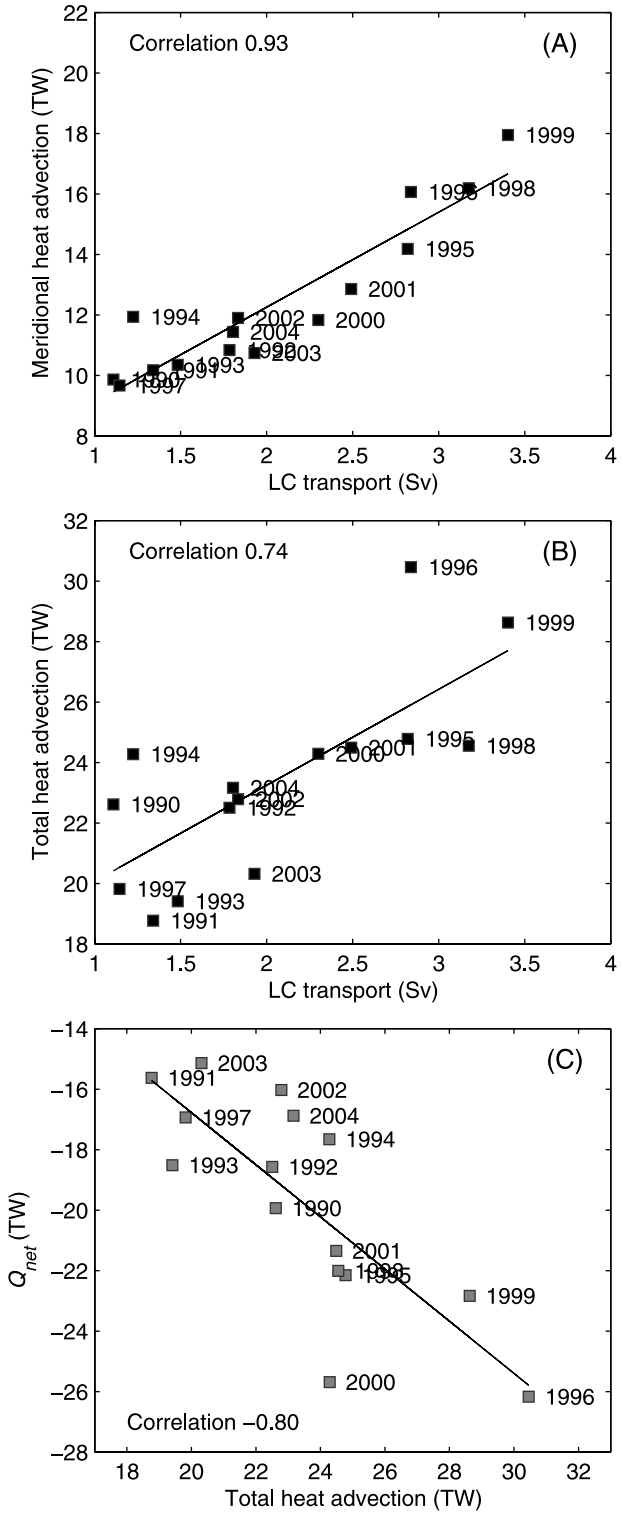

Figure 12. Relationships between the annual mean Leeuwin Current transport with the (a) meridional and (b) total heat advection into the control volume off the west coast of Australia and (c) relationship between annual mean total heat advection and air-sea heat flux (Q_{net}). The solid lines are linear regressions between the variables.

and the net air-sea heat loss (Figure 11 (bottom)). Note the net air-sea heat loss is highly correlated with the latent heat flux (correlation 0.95; not shown). The two-month phase lag could be a reflection of the advection timescales: assuming an average speed of 10 cm s^{-1}, it takes about two months for the Leeuwin Current waters entering at 27°S to leave the control volume at 32°S; it takes about 2–3 months for the Leeuwin Current warm core eddies to detach and move westward across 110°E [*Fang and Morrow*, 2003; *Feng et al.*, 2007]. The combination of total heat advection and Q_{net} anomalies explains more than 60% of the interannual heat content variation in the Leeuwin Current region.

[23] During 1990–2004, the correlation between the annual mean Leeuwin Current transport at 32°S and the total heat advection (meridional advection) is 0.74 (0.93) (Figures 12a and 12b), both above 99% significance level. The slopes from linear regressions reveal that the heating rates of the meridional and total advection change by 3.1 and 3.2 TW for 1-Sv increment in the Leeuwin Current transport at 32°S. On annual average, 1996 and 1999 have relative high air-sea heat loss when the heat advection is strong (Figure 12c). The high air-sea heat loss during 2000, when the total heat advection is not as strong, may be partly related to the higher model SST in 2000 compared to observation (Figure 7). During 1990–2004, the annual mean values of the total advection and Q_{net} have a linear correlation of −0.8. Note variation in large-scale winds may also affect the air-sea heat flux in the subtropical Indian Ocean off the Australian coast [*England et al.*, 2006].

6. Temperature Variation in February–April

6.1. Background

[24] *Caputi et al.* [2001] indicated that the positive water temperature anomalies in the Leeuwin Current region in February–April may improve the larval survival and growth of the western rock lobster during years of stronger Leeuwin Current. The western rock lobster spawns from November to February on the shelf in depths of about 40–100 m and the larvae are transported offshore by wind-driven currents during the austral summer. Surveys of larval distribution have shown good abundance of larvae out to 105°E [*Phillips*, 1981], so that during the February–April period there would be a high proportion of early stage larvae in the Leeuwin Current region. These larvae are transported back to the coast and settle in the inshore coastal areas during the puerulus (postlarval) stage from August to December. The advection effect of the Leeuwin Current in June–December has been shown to strongly affect ($r = 0.86$, $p < 0.001$) the spatial distribution of the puerulus settlement [*Caputi*, 2008]. The level of puerulus settlement significantly affects the legal catch 3–4 years later.

6.2. Temperature Variation

[25] The interannual variation of SST in February–April is shown to have a linear correlation of 0.77 (1982–1999) with the annual mean Fremantle sea level [*Caputi et al.*, 2001]. From a lag correlation analysis (Figure 13), the significant correlation between the February–April SST and monthly Fremantle sea level is mostly evident for the February–May period. The correlation between SST and Southern Oscillation Index is lower (Figure 13), indicating

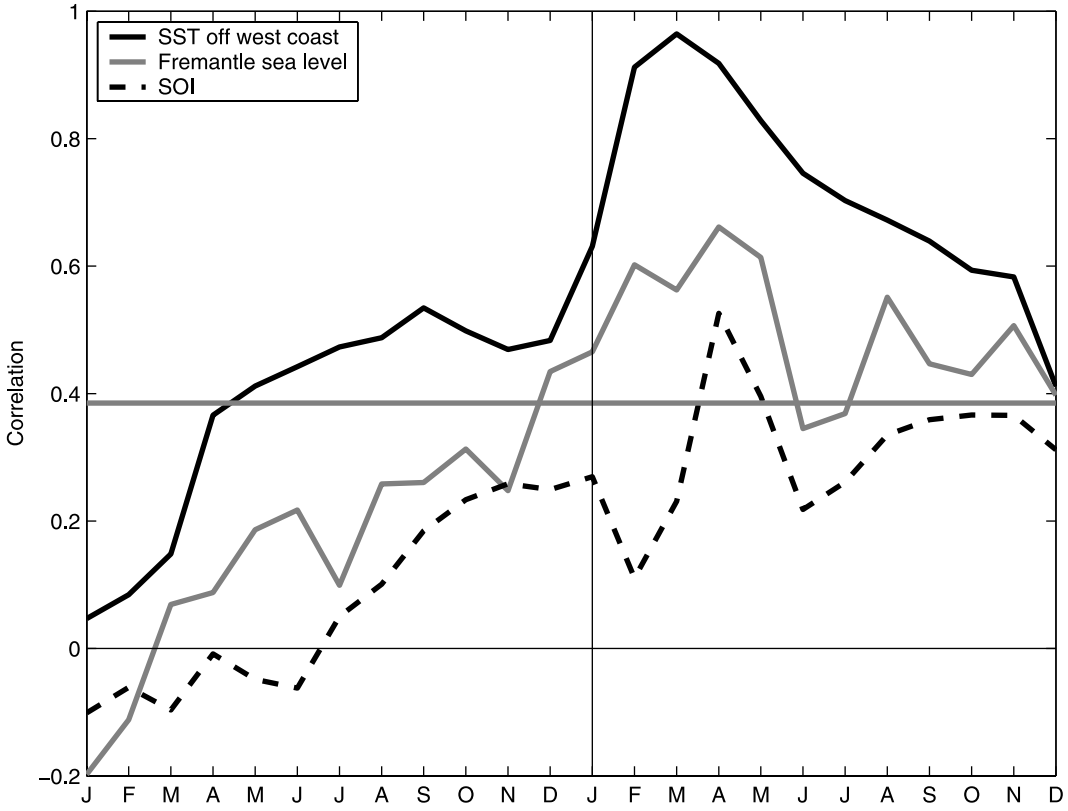

Figure 13. Lag correlation between the average February–April ORCA025 SST off the west coast of Australia with the monthly SST from ORCA025 in the same region, Fremantle sea level from observation, and the Southern Oscillation Index of the current and previous years during 1961–2004. The horizontal gray line denotes the 99% significance levels of the correlations by assuming 42° of freedom.

that the ENSO teleconnection may not significantly influence SST in the region. ORCA025 captures most of the interannual variation in the February–April mean SST off the west coast during 1990–2004, and the correlation between the modeled and observed February–April SST is 0.95 (Figure 7 (bottom)).

6.3. Heat Budget

[26] Marginally significant correlations (~0.5) of February–April SST anomaly and monthly SST off the west coast of Australia extends to the previous austral winter (Figure 13), indicating that the ocean memory of temperature anomaly from the winter season, when the mixed layer depth is deep, may play a role to determine the February–April SST anomaly. The correlation between the average February–April SST anomalies and that of the previous September–November average is 0.73, so that the signs of SST anomalies in September–November usually determine the signs of SST anomalies in February–April of the following year. Note that the interannual variation of February–April average SST (standard deviation: 0.67°C) is about 60% higher than that of September–November average. The lowest February–April SST anomaly is observed in 1993 (−1.1°C) during an El Nino event, and the highest is observed in 2000 (1.3°C) during an extended La Nina event. In both events, there are significant temperature anomalies (~0.5°C) during the previous austral winters (Figure 14).

[27] The upper ocean heat budget integration during 1990–2004 indicates that the heat advection and air-sea flux also influence the interannual variations of February–April SST in the Leeuwin Current region (Figure 14). In about half of the years during this period, the total heat advection determines the signs of SST anomalies in February–April (correlation 0.75). The contributions from surface heat flux and advection usually have opposite signs, indicating the air-sea flux acts as a buffer to the interannual SST variations in the Leeuwin Current region.

6.4. Discussion

[28] The interannual variation of the average February–April surface temperature off the west coast of Australia, which is crucial for western rock lobster recruitment, is mainly controlled by the Leeuwin Current heat advection as well as the ocean memory from the previous austral winter, with the air-sea flux playing a buffering role. While warmer SST may increase the growth rate of the lobster larvae during their early phase so that improve their survival rates [*Caputi et al.*, 2008], the physical processes that control the SST anomaly may also have indirect contributions to the recruitment process. A stronger Leeuwin Current would increase vertical mixing in the upper ocean (because of surface heat loss) so that enhance regional nutrient supply

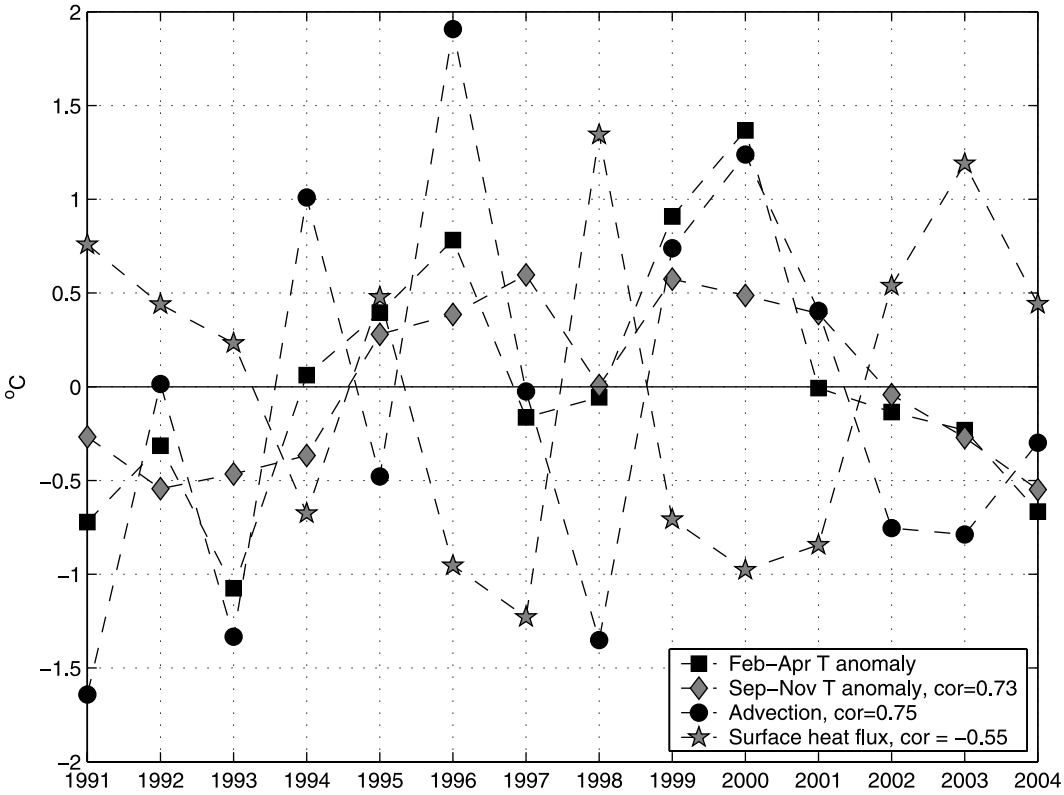

Figure 14. Surface layer temperature anomalies in the Leeuwin Current region during February–April and the previous September–November and the temporal integrations of the total heat advection and the air-sea heat flux terms in the heat balance equation from previous October–March during 1991–2004. The correlations with the February–April average temperature anomalies are shown in the legend box, which are all above 95% significant level.

and primary production (M. Feng et al., submitted manuscript, 2008), which may have a positive effect on larval survival rate and then recruitment.

7. Summary

[29] In this study, monthly output from an eddy-resolving numerical model, ORCA025, has been used to understand the seasonal and interannual variations of upper ocean heat balance in the Leeuwin Current region during 1990–2004. ORCA025 has captured the seasonal and interannual variations of the Leeuwin Current and regional SST reasonably well, when compared with historical and satellite altimeter data analyses.

[30] There is enhanced latent heat flux in the Leeuwin Current region compared to the offshore region at the same latitude. On seasonal cycle, both the volume transport and heat advection of the Leeuwin Current are stronger during the austral winter and weaker during the austral summer, and the heat budget off the west coast of Australia is predominantly balanced by the seasonal variations of the Leeuwin Current heat advection and the net air-sea heat exchange.

[31] On the interannual timescale, both the volume transport and heat advection of the Leeuwin Current are stronger during a La Niña event and weaker during an El Niño event, and the heat balance is also primarily determined by the variations of heat advection and the air-sea heat flux, with the heat advection variation leading the opposite air-sea (latent) heat flux variation by two months. While the two-month time lag is likely due to the advection timescale of the Leeuwin Current and its eddies, the significant negative correlations between the annual mean Leeuwin Current heat advection and the latent and net heat fluxes in the Leeuwin Current region indicates that the variation of the Leeuwin Current heat advection may determine the variation of the latent heat release in the Leeuwin Current region.

[32] The February–April SST anomalies off the west coast of Australia, which are important for the western rock lobster recruitment off the coast, are dominantly affected by the Leeuwin Current advection as well as the SST memory from the previous winter, and are buffered by variations in the net air-sea heat flux.

[33] **Acknowledgments.** This research is supported by the Western Australia Marine Science Institution and the CSIRO Wealth from Oceans National Research Flagship. We would thank two anonymous reviewers for helpful comments.

References

Adcroft, A., C. Hill, and J. Marshall (1997), Representation of topography by shaved cells in a height coordinate ocean model, *Mon. Weather Rev.*, *125*, 2293–2315, doi:10.1175/1520-0493(1997)125<2293:ROTBSC>2.0.CO;2.

Alory, G., S. Wijffels, and G. Meyers (2007), Observed temperature trends in the Indian Ocean over 1960–1999 and associated mechanisms, *Geophys. Res. Lett.*, *34*, L02606, doi:10.1029/2006GL028044.

Barnier, B., et al. (2006), Impact of partial steps and momentum advection schemes in a global ocean circulation model at eddy permitting resolution, *Ocean Dyn.*, *56*(5–6), 543–567, doi:10.1007/s10236-006-0082-1.

Birol, F., and R. Morrow (2003), Separation of quasi-semiannual Rossby waves from the eastern boundary of the Indian Ocean, *J. Mar. Res.*, *61*, 707–723, doi:10.1357/002224003322981110.

Caputi, N. (2008), Impact of the Leeuwin Current on the spatial distribution of the puerulus settlement of the western rock lobster (*Panulirus cygnus*) fishery of Western Australia, *Fish. Oceanogr.*, *17*, 147–152, doi:10.1111/j.1365-2419.2008.00471.x.

Caputi, N., C. F. Chubb, and A. Pearce (2001), Environmental effects on recruitment of the western rock lobster, *Panulirus cygnus*, *Mar. Freshwater Res.*, *52*, 1167–1175, doi:10.1071/MF01180.

Caputi, N., S. de Lestang, M. Feng, and A. Pearce (2008), Seasonal variation in the long-term warming trend in water temperature off the Western Australian coast, *Mar. Freshwater Res.*, in press.

Cresswell, G. R., and T. J. Golding (1980), Observations of a south-flowing current in the southeastern Indian Ocean, *Deep Sea Res., Part A*, *27*, 449–466, doi:10.1016/0198-0149(80)90055-2.

Domingues, C. M., S. E. Wijffels, M. E. Maltrud, J. A. Church, and M. Tomczak (2006), The role of eddies in cooling the Leeuwin Current, *Geophys. Res. Lett.*, *33*, L05603, doi:10.1029/2005GL025216.

Du, Y., and S.-P. Xie (2008), Role of atmospheric adjustments in the tropical Indian Ocean warming during the 20th century in climate models, *Geophys. Res. Lett.*, *35*, L08712, doi:10.1029/2008GL033631.

England, M. H., C. C. Ummenhofer, and A. Santoso (2006), Interannual rainfall extremes over southwest Western Australia linked to Indian Ocean climate variability, *J. Clim.*, *19*, 1948–1969, doi:10.1175/JCLI3700.1.

Fang, F., and R. Morrow (2003), Evolution, movement and decay of warm-core Leeuwin Current eddies, *Deep Sea Res., Part II*, *50*, 2245–2261, doi:10.1016/S0967-0645(03)00055-9.

Feng, M., and G. Meyers (2003), Interannual variability in the tropical Indian Ocean: A two-year timescale of Indian Ocean Dipole, *Deep Sea Res., Part II*, *50*, 2263–2284, doi:10.1016/S0967-0645(03)00056-0.

Feng, M., P. Hacker, and R. Lukas (1998), Upper ocean heat and salt balances in response to a westerly wind burst in the western equatorial Pacific during TOGA COARE, *J. Geophys. Res.*, *103*, 10,289–10,311, doi:10.1029/97JC03286.

Feng, M., G. Meyer, A. Pearce, and S. Wijffels (2003), Annual and interannual variations of the Leeuwin Current at 32°S, *J. Geophys. Res.*, *108*(C11), 3355, doi:10.1029/2002JC001763.

Feng, M., S. Wijffels, J. S. Godfrey, and G. Meyers (2005), Do eddies play a role in the momentum balance of the Leeuwin Current?, *J. Phys. Oceanogr.*, *35*, 964–975, doi:10.1175/JPO2730.1.

Feng, M., L. J. Majewski, C. B. Fandry, and A. M. Waite (2007), Characteristics of two counter-rotating eddies in the Leeuwin Current system off the Western Australian coast, *Deep Sea Res., Part II*, *54*, 961–980, doi:10.1016/j.dsr2.2006.11.022.

Godfrey, J. S., and K. R. Ridgway (1985), The large-scale environment of the poleward-flowing Leeuwin Current, Western Australia: Longshore steric height gradients, wind stresses, and geostrophic flow, *J. Phys. Oceanogr.*, *15*, 481–495, doi:10.1175/1520-0485(1985)015<0481:TLSEOT>2.0.CO;2.

Large, W. G. (2007), Core forcing for coupled ocean and sea ice models, *Flux News*, *3*, 2–3.

Large, W., and S. Yeager (2004), Diurnal to decadal global forcing for ocean and sea ice models: The data sets and flux climatologies, *Tech. Note NCAR/TN–460+STR*, Clim. and Global Dyn. Div. of the Natl. Cent. for Atmos. Res., Boulder, Colo.

Lee, T., I. Fukumori, and B. Tang (2004), Temperature advection: Internal versus external processes, *J. Phys. Oceanogr.*, *34*, 1936–1944, doi:10.1175/1520-0485(2004)034<1936:TAIVEP>2.0.CO;2.

Le Traon, P. Y., F. Nadal, and N. Ducet (1998), An improved mapping method of multi-satellite altimeter data, *J. Atmos. Oceanic Technol.*, *15*, 522–534, doi:10.1175/1520-0426(1998)015<0522:AIMMOM>2.0.CO;2.

Madec, G. (2007), NEMO: The OPA ocean engine, note pole modélisation, Inst. Pierre-Simon Laplace, Paris.

Meyers, G. (1996), Variation of Indonesian throughflow and the El Nino–Southern Oscillation, *J. Geophys. Res.*, *101*, 12,255–12,263.

Pearce, A., and M. Feng (2007), Observations of warming on the Western Australian continental shelf, *Mar. Freshwater Res.*, *58*, 914–920, doi:10.1071/MF07082.

Pearce, A. F., and B. F. Phillips (1988), ENSO events, the Leeuwin Current and larval recruitment of the western rock lobster, *J. Cons. Cons. Int. Explor. Mer*, *45*(1), 13–21.

Phillips, B. F. (1981), The circulation of the southeastern Indian Ocean and the planktonic life of the western rock lobster, *Oceanogr. Mar. Biol.*, *19*, 11–39.

Rayner, N. A., D. E. Parker, E. B. Horton, C. K. Folland, L. V. Alexander, D. P. Rowell, E. C. Kent, and A. Kaplan (2003), Global analyses of sea surface temperature, sea ice, and night marine air temperature since the late nineteenth century, *J. Geophys. Res.*, *108*(D14), 4407, doi:10.1029/2002JD002670.

Reason, C. J. C., D. Gamble, and A. F. Pearce (1999), The Leeuwin Current in the parallel ocean climate model and applications to regional meteorology and fisheries, *Meteorol. Appl.*, *6*, 211–225, doi:10.1017/S1350482799001255.

Shinoda, T., and H. H. Hendon (2001), Upper-ocean heat budget in response to the Madden–Julian Oscillation in the western Equatorial Pacific, *J. Clim.*, *14*, 4147–4165, doi:10.1175/1520-0442(2001)014<4147:UOHBIR>2.0.CO;2.

Smith, R. L., A. Huyer, J. S. Godfrey, and J. Church (1991), The Leeuwin Current off Western Australia, 1986–1987, *J. Phys. Oceanogr.*, *21*, 323–345, doi:10.1175/1520-0485(1991)021<0323:TLCOWA>2.0.CO;2.

Smith, T. M., and R. W. Reynolds (2004), Improved extended reconstruction of SST (1854–1997), *J. Clim.*, *17*, 2466–2477.

Trenberth, K. E., J. G. Olson, and W. G. Large (1989), A global ocean wind stress climatology based on ECMWF analyses, *Rep. NCAR/TN-338+STR*, Natl. Cent. for Atmos. Res, Boulder, Colo.

Wentz, F. J. (1997), A well-calibrated ocean algorithm for SSM/I, *J. Geophys. Res.*, *102*, 8703–8718, doi:10.1029/96JC01751.

A. Biastoch and C. Böning, Leibniz-Institut für Meereswissenschaften, Düsternbrooker Weg 20, D-24105 Kiel, Germany.

N. Caputi, Western Australian Fisheries and Marine Research Laboratories, Department of Fisheries, P.O. Box 20, North Beach, WA 6920, Australia.

M. Feng, CSIRO Marine and Atmospheric Research, Underwood Avenue, Floreat, WA 6014, Australia. (ming.feng@csiro.au)

G. Meyers, Integrated Marine Observing System, University of Tasmania, Hobart, TAS 7001, Australia.